Stochastic control of wave energy converters for optimal power absorption with constrained control force

Sun, Tao; Nielsen, Søren R.K.

Published in:
Applied Ocean Research

DOI (link to publication from Publisher):
10.1016/j.apor.2019.03.002

Publication date:
2019

Document Version
Early version, also known as pre-print

Contents lists available at ScienceDirect

Applied Ocean Research

journal homepage: www.elsevier.com

Stochastic control of wave energy converters for optimal power absorption with constrained control force

Tao Sun *, Søren R.K. Nielsen

Department of Civil Engineering, Aalborg University, 9000 Aalborg, Denmark

ARTICLE INFO

MSC:
00-01
99-00

Keywords:
Wave energy
Heave point absorber
Optimal power take-off
Actuator force constraints

ABSTRACT

This paper presents an analytical solution derived for optimal control of the power take-off of a single-degree of freedom heave point absorber with constraints on the control force. The optimal control law turns out to be noncausal with a functional dependence on future velocities. To handle this problem, an algorithm for predicting future velocities is derived. Based on the solution the mean (time-averaged) absorbed power in a given sea-state is calculated. The performance of the indicated controller in terms of the mean absorbed power is close to the optimal value obtained by nonlinear programming and better than a controller with feedback from the present displacement, velocity and acceleration, and with optimized gain factors.

1. Introduction

The heave wave energy point absorber is assumed to be constrained by a mooring system or otherwise to enforce a motion only in the vertical direction, and hence the absorber can be modelled as a single-degree-of-freedom oscillator driven by the external wave load.

Significant increase of the power take-off (PTO) of a heave absorber may be achieved by using an active vibration control of the vertical motion [1]. In order to obtain a maximal absorbed power, many studies have proposed control strategies for wave energy converters. Latching control is the most investigated control strategy, independently proposed by Falnes [2] and French [3]. If the velocity and wave load have different signs, so that the wave force supplies a negative power to the device, the absorber is fixed at zero velocity ('latched') by an external mechanism. Hence, the control effort is based on the observation of the wave load and the velocity of the absorber, and hence may be classified as a mixed feedback and feedforward control strategy. For an induction (asynchronous) generator, where the power takeoff force is proportional to the velocity of the absorber, a positive power takeoff is always achieved during the unlatched state. Hoskin and Nichols [4] proved the basic assumption of the latching control strategy to be optimal during the unlatched periods for an induction generator. Subsequently, latching control has been extended to multi-degree-of-freedom wave energy converters [5,6]. Babarit et al. [7] have suggested a somewhat similar semi-active control strategy, known as declutching, where the generator is cut off when the wave force and the absorber velocity are out of phase. Both control strategies require the external wave load to be estimated. Assuming a linear wave theory, this is given as a noncausal convolution of the surface elevation, i.e. there is a need to predict future surface elevations a certain control horizon ahead of the time when the control is applied. This is easy for regular waves or narrow-banded sea states, but the accuracy of the prediction may be affected in broad-banded irregular sea states.

To circumvent the uncertainties related with open-loop control robust closed loop control law in term of classical PID control have been suggested by Astrom and Hagglund [8]. Typically, the control laws will introduce negative control stiffness in order to make the system more flexible [9]. Nielsen et al. [10] derived the optimal control law in the time domain for a heave point absorber with non-linear buoyancy or restoring forces from the mooring system in case of no constraints on the displacements and the control force. The control law is a feedback type depending on the present displacement and acceleration of the absorber and an integral feedback from future velocities. Hence, for practical applications, the indicated control law requires a prediction of future velocities. Because there is no dependence on the wave load, the indicated control law applies to both 2D and 3D irregular sea-states.

* Corresponding author.
Email addresses: tsu@civil.aau.dk (T. Sun); srkn@civil.aau.dk (S.R.K. Nielsen)

https://doi.org/10.1016/j.apor.2019.03.002
Received 6 May 2018; Received in revised form 28 February 2019; Accepted 4 March 2019
Available online xxx

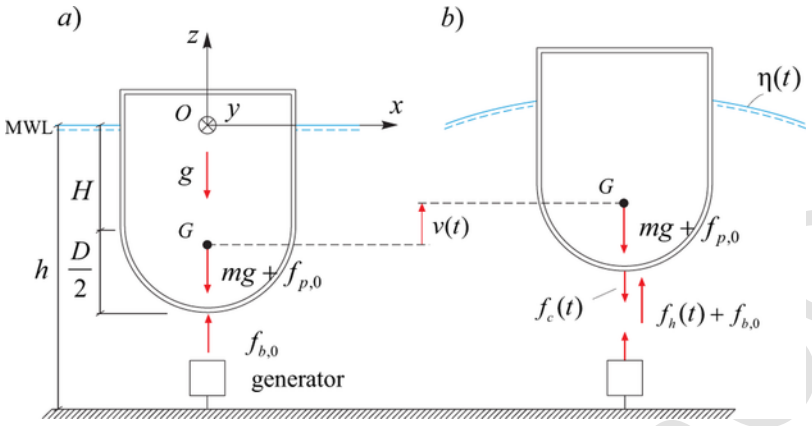

Fig. 1. Loads on heave absorber. (a) Static equilibrium state. (b) Dynamic state.

Table 1
Heave absorber and wave excitation parameters.

Parameter	Value	Unit	Parameter	Value	Unit
H	7.00	m	H_s	3.00	m
D	14.00	m	T_p	7.42	s
h	30.00	m	γ	5	
m	1.84×10^6	kg	$\sigma_{\dot{v}}$	2.9991	m/s
m_h	0.44×10^6	kg	$\sigma_{f_{c,0}}$	1.8645×10^6	N
k	1.51×10^6	N/m	$P_{\text{opt},0}$	7.2347×10^5	W
β_1	0.82		β_2	0.80	
c	1.0×10^5	kg/s			

Displacement constraints may also be imposed to prevent the absorber from hitting the sea-bottom or jumping out of the water, which may lead to damaging impact loadings. Similarly, constraints may be present on the control force due to saturation in the actuator system or in order to reduce structural fatigue damage accumulation in hot spots in the absorber shell structure. Hansen and Kramer [11] considered constraints on the control force of a WaveStar point converter based on a PD reactive control law and concluded that the constraint significantly influences the mean absorbed power and changes the values of the optimal gain factors of the PD controller. Based on the Pontryagin maximum principle, Hendrikx et al. [12] considered the open-loop optimal control strategy for a WaveStar point absorber with constraints on the control torque. The difference of absorbed power between optimal control and model predictive control strategy was small but the control torque trajectory differed.

A variety of model predictive control (MPC) formulations with the constraints on the state vector and the control force have been reported in the literatures [13,14]. Soltani et al. [15] derived an MPC algorithm to maximize the absorbed power of a Wavestar wave energy converter. The main prerequisite is that the absorber velocity shall be in phase with the wave load. Hence, the controller needs prediction of the future sea state and observation of the absorber velocity.

A recent variation of the general model predictive control (MPC) framework has been suggested by Bacelli and Ringwood [16]. Based on spectral and pseudospectral optimal control methods, the WEC responses and control force are expanded on a functional basis, resulting in a computationally efficient formulation. The spectral method is based on truncated Fourier series, leading to a convex optimization problem and an effective solution for the optimal control. Afterward, Genest and Ringwood [17] developed a receding horizon real-time pseudospectral control algorithm for a wave energy converter with constraints on displacement and control force. The functional basis consists of half-range Chebyshev Fourier functions, which can repre-

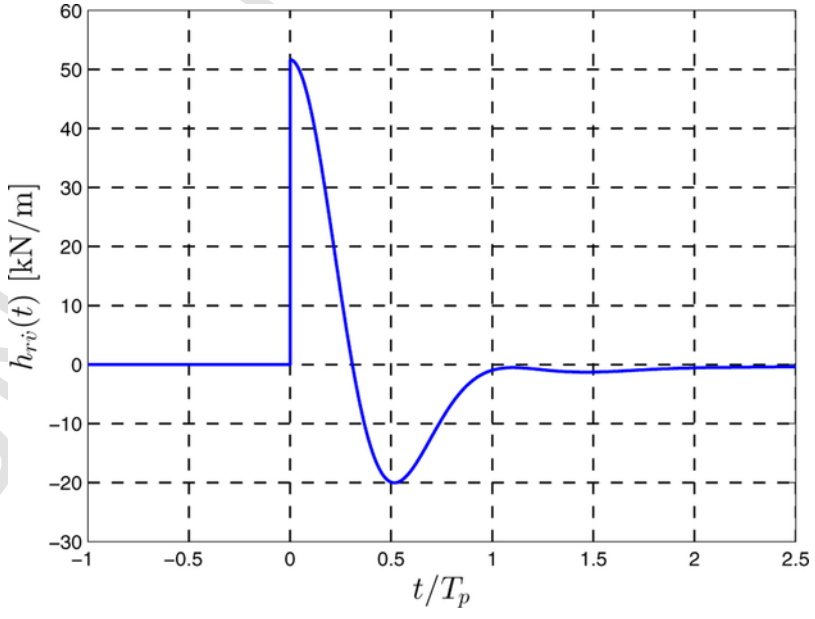

Fig. 2. Impulse response function for the radiation force, $h_{r\dot{v}}(t)$.

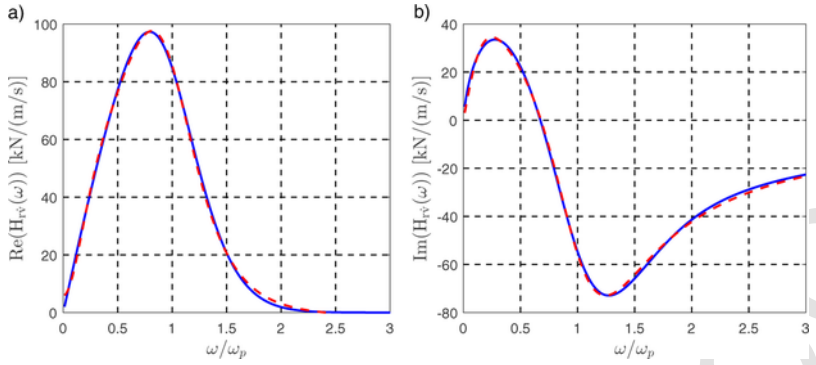

Fig. 3. Frequency response function for the radiation force. (a) $\mathrm{Re}(\mathrm{H}_{\dot{v}\dot{v}}(\omega))$. (b) $\mathrm{Im}(\mathrm{H}_{\dot{v}\dot{v}}(\omega))$: Numerical determined target. - - -: Rational approximation with order $(m, n) = (2, 3)$.

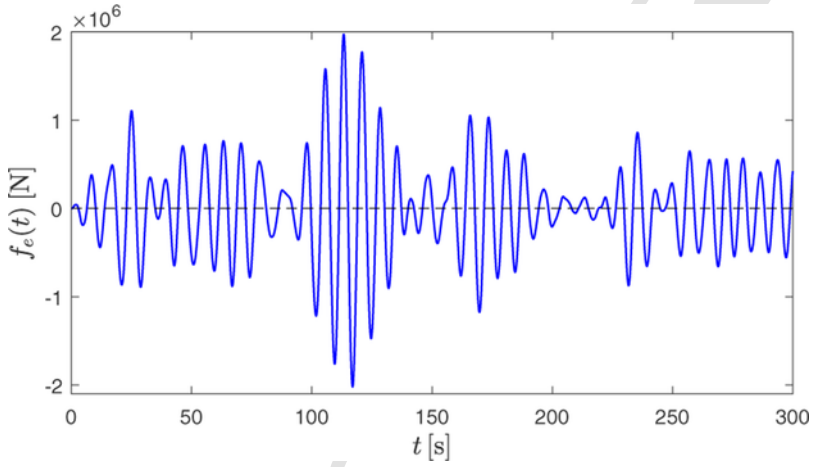

Fig. 4. Realization of the wave load process $f_e(t)$. $H_s = 3\,\mathrm{m}$, $T_p = 7.42\,\mathrm{s}$, $\gamma = 5$.

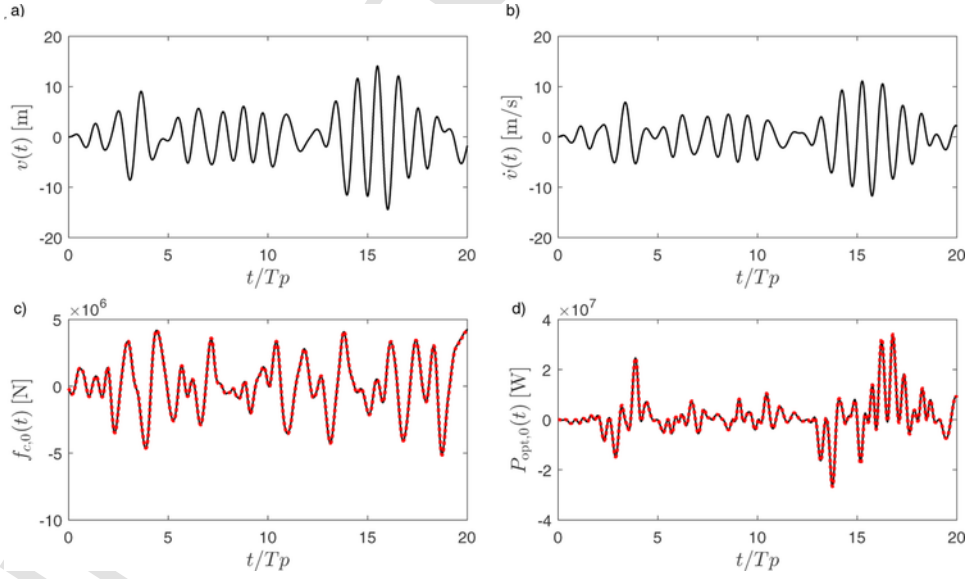

Fig. 5. Unconstrained case, optimal trajectories and power take-off. (a) $v(t)$. (b) $\dot{v}(t)$. (c) $f_{c,0}(t)$. (d) $P_{\mathrm{opt},0}(t)$. —: Nonlinear programming solution. ⋯⋯: Unconstrained analytical solution.

sent the harmonic signals in the application domain well. Further, the receding horizon is introduced to the control algorithm in order to effectively deal with the signal truncation effects. Compared with alternative MPC formulations, pseudospectral control algorithm shows considerable promise in achieving a good balance between performance and computation.

The present paper presents an analytical solution for the optimal control of a heave point absorber with constraints on the control force. The control law has feedback from present displacement and acceleration and future velocities, which need to be predicted. The obtained control law has been benchmarked against the optimal control ob-

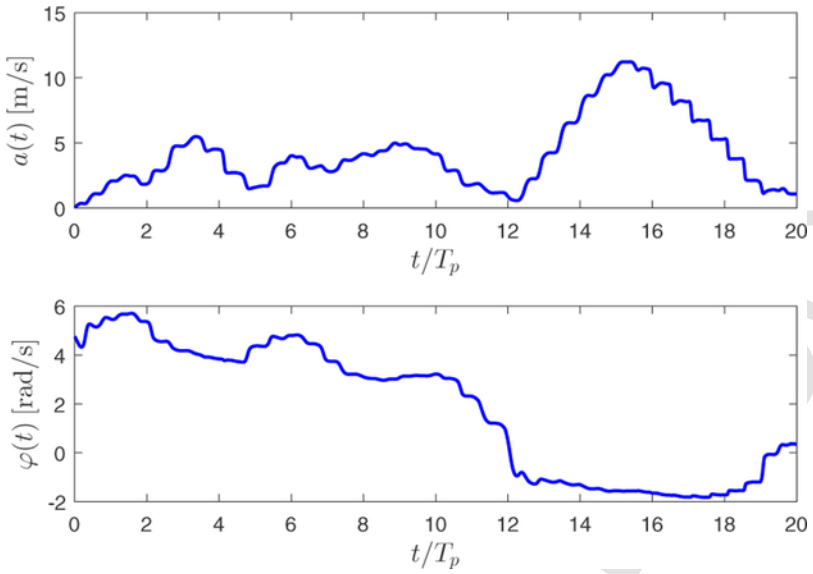

Fig. 6. Constrained control force ($f_{c,\max} = -f_{c,\min} = 2 \times 10^6$ N) and unconstrained displacement. (a) v(t). (b) $\dot{v}$(t). (c) $f_c(t)$. (d) $P(t)$. —: Nonlinear programming solution. ⋯⋯: Eq. (34).

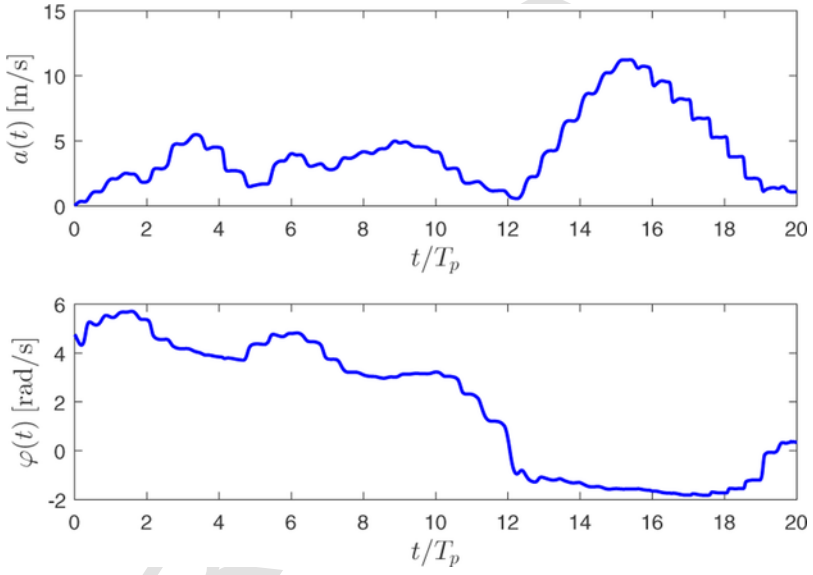

Fig. 7. Realizations of amplitude $a(t)$ and phase $\varphi(t)$ for the unconstrained absorber.

tained from a nonlinear programming algorithm indicated in the appendix to the paper.

The paper is organised as follows. Section 2.1 presents the basic equations of the problem, and the inherent approximations in the nonlinear programming algorithm is justified by comparison to the theoretical unconstrained solution obtained by Nielsen et al. [10]. Section 2.2 derives the optimal control law for a point absorber with constraints on the control force, and the obtained solution is benchmarked against numerical obtained nonlinear programming solution. The obtained control law has feedback from further velocities. For wave energy converters, even if the external wave load is broad-banded, the response is relatively narrow-banded. Therefore, a van der Pol transformation [18] with slowly varying amplitude and phase has been used for the prediction of future velocities in Section 2.3. Section 2.4 derives the analytical mean absorbed power with the constraints on the control force in a given sea-state described by the significant wave height, the peak period and a band-width parameter. Section 3 investigates the performance of the proposed control method, which is compared with the nonlinear programming solution and a causal controller with feedback from the present displacement, velocity and acceleration.

2. Methodology

2.1. Equation of motion of point absorber

Fig. 1 shows the heave absorber to be analyzed. An (x, y, z)-coordinate system is introduced with the origin O placed in the mean water level (MWL) at the centerline of the point absorber. The horizontal x-axis is orientated in the direction of the wave propagation, and the vertical z-axis is orientated in the upward direction. Only two-dimensional (plane) irregular waves are considered. The motion v(t) of the body in the z-direction is measured from the static equilibrium state, where the static buoyancy force $f_{b,0}$ balances the gravity force mg and a possible static pre-stressing force from the mooring system $f_{p,0}$. g is the acceleration of gravity, and m indicates the structural mass including ballast. The center of gravity is denoted G.

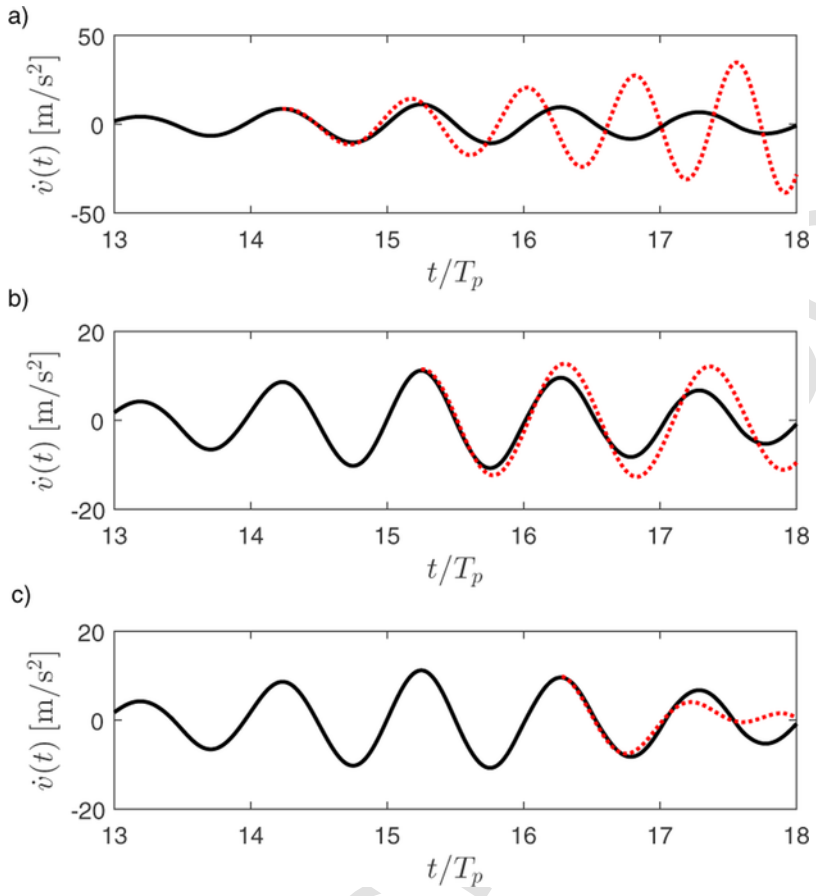

Fig. 8. Prediction of $\dot{v}(t)$. (a) $t = 14.25T_p$. (b) $t = 15.25T_p$. (c) $t = 16.25T_p$. —: Nonlinear programming solution. ·····: Prediction velocity response.

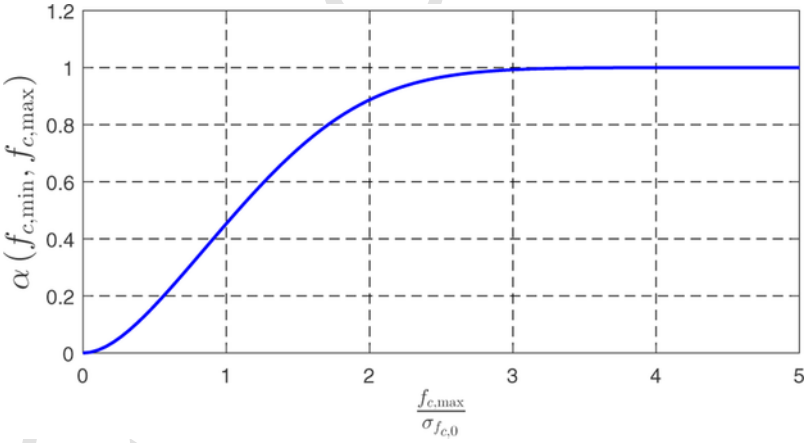

Fig. 9. Reduction coefficient $\alpha\,(f_{c,\min}, f_{c,\max})$ as a function of $\frac{f_{c,\max}}{\sigma_{f_{c,0}}}$, $f_{c,\min} = -f_{c,\max}$.

In the dynamic state caused by the surface elevation $\eta(t)$, the WEC is excited by an additional dynamic hydrodynamic force $f_h(t)$ and an additional force, $f_c(t)$, from an external hydraulic or electric force generator as the PTO system, which is used to control the motion of the absorber. $f_c(t)$ is considered positive in the opposite direction of $v(t)$, and will be referred to as the control force. In realistic application, the efficiency of the actuator will be smaller than 100% due to energy losses and actuators efficiency influencing the control performance when the large amount of reactive power is involved [19]. In theoretical research, it is assumed that the actuator has ideal efficiency and an ideal PTO system is applied. Further, a PTO system can provide the reactive power. In applications, the cylinder in the PTO system can operate as a pump, producing a bi-directional flow, which drives a hydraulic motor. The motor adapts to the flow and rectifies the flow into a unidirectional turning of the generator. Further, the PTO system absorbs a positive power from the absorber if the control force and the velocity are in counter phase i.e. the actuator is working as a damper. In the other way, the PTO system acts as a motor and supplies energy to the absorber. Assuming linear wave theory, $f_h(t)$ may be written as a superposition of the following contributions:

$$f_h(t) = f_b(t) + f_r(t) + f_e(t) \tag{1}$$

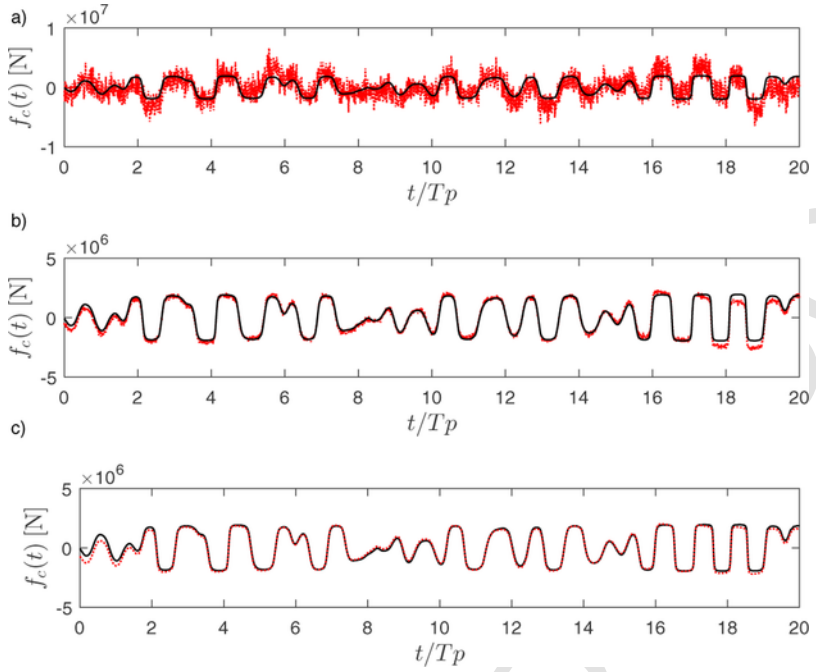

Fig. 10. Comparison of control force $f_c(t)$ with different noise level on the observation of the acceleration singal. (a) $a_1 = 0.5\,\mathrm{m/s^{1/2}}$. (b) $a_1 = 0.05\,\mathrm{m/s^{1/2}}$. (c) $a_1 = 0.001\,\mathrm{m/s^{1/2}}$. —: Nonlinear programming solution. - - -: Noise affected solution.

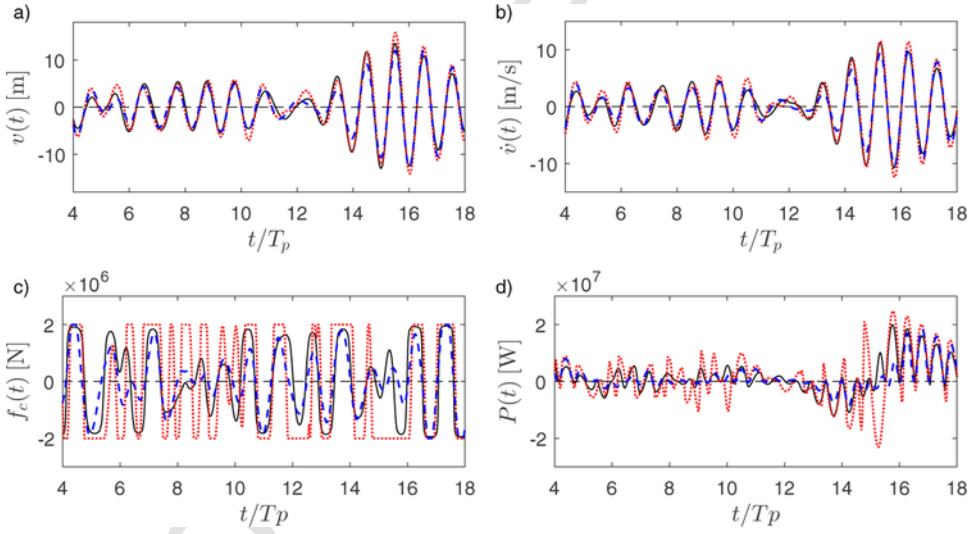

Fig. 11. Realization 1: Comparison of trajectories for different control strategies. —: Nonlinear programming solution. ·····: $f_{c,0}(t)$ given by Eq. (33). - - -: $f_{c,0}(t)$ given by Eq. (57).

where $f_b(t)$ is the quasi-static restoring force from the static equilibrium state of the buoyancy and the mooring system, $f_r(t)$ is the radiation force generated by the motion of the absorber in still water, and $f_e(t)$ is the wave excitation force caused by the wave action, when the absorber is fixed in the static equilibrium state. The term $f_r(t)$ removes mechanical energy from the absorber by generating an outwards directed radial wave train, whereas $f_e(t)$ supplies energy to the absorber.

$f_b(t)$ may be written as an analytical nonlinear function of the displacement:

$$f_b(\mathrm{t}) = -\mathrm{r}(\mathrm{v}(\mathrm{t})) \tag{2}$$

Assuming small vertical vibrations, Eq. (2) may be linearized around the static equilibrium state as [20]:

$$f_b(\mathrm{t}) = -\mathrm{k}\,\mathrm{v}(\mathrm{t}) \quad , \mathrm{k} = \mathrm{r}'(0) \tag{3}$$

In the numerical results below the linearized relation in Eq. (3) has been assumed with the value of k given in Table 1 below.

The radiation force $f_r(t)$ may be written in terms of the following differential-integro relation [21,22]:

$$f_r(\mathrm{t}) = -m_h\ddot{\mathrm{v}}(\mathrm{t}) - \mathrm{f}_{\mathrm{r},0}(\mathrm{t}) \tag{4}$$

$$\mathrm{f}_{\mathrm{r},0}(\mathrm{t}) = \int_{\mathrm{t}_0}^{\mathrm{t}} \mathrm{h}_{\mathrm{r}\dot{\mathrm{v}}}(\mathrm{t}-\tau)\dot{\mathrm{v}}(\tau)\,d\tau \tag{5}$$

where m_h indicates the added water mass at infinite high frequencies, and $\mathrm{h}_{\mathrm{r}\dot{\mathrm{v}}}(\mathrm{t})$ is a causal impulse response function for the radiation force brought forward by the absorber velocity $\dot{\mathrm{v}}(\tau)$. t_0 is the initial time of the control.

Due to the causality of the impulse response function, the related frequency response function becomes:

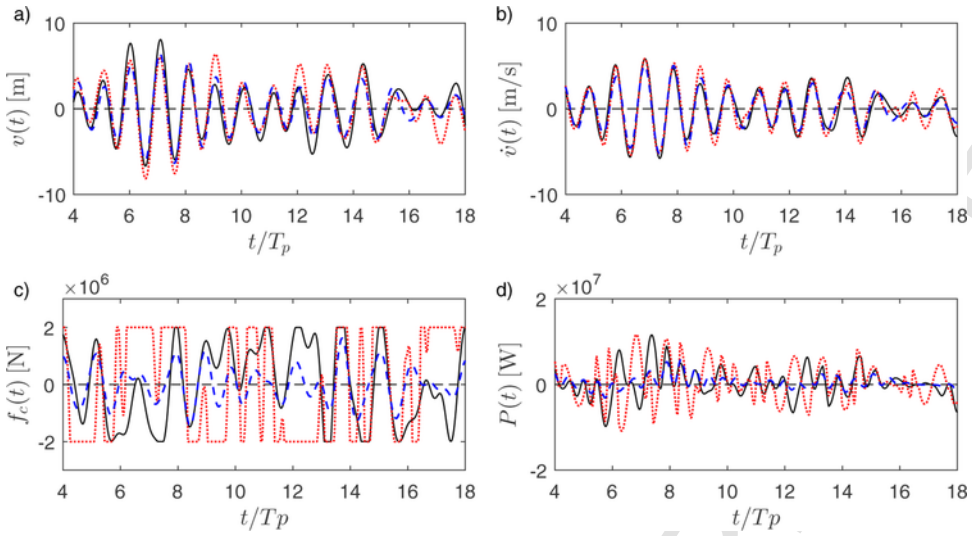

Fig. 12. Realization 2: Comparison of trajectories for different control strategies. —: Nonlinear programming solution. ·····: $f_{c,0}(t)$ given by Eq. (33). – – –: $f_{c,0}(t)$ given by Eq. (57).

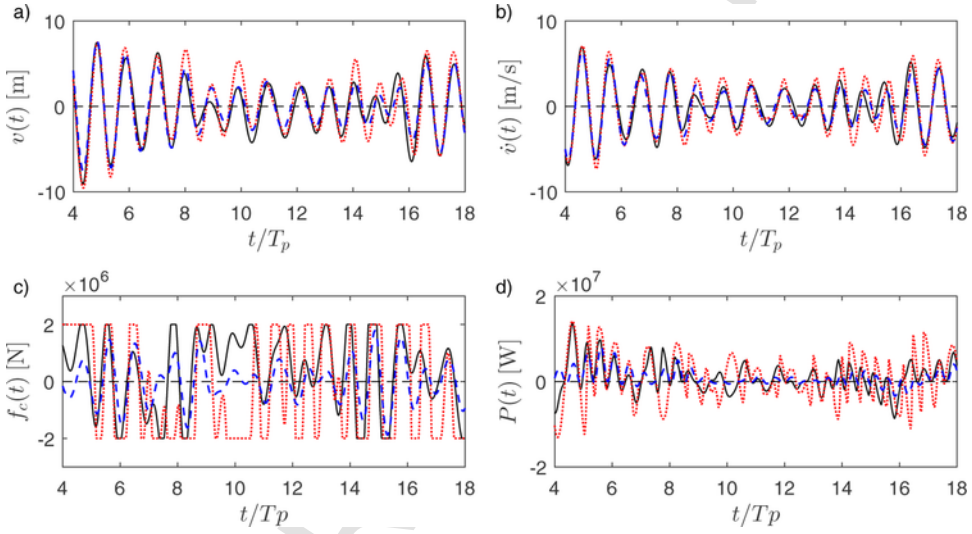

Fig. 13. Realization 3: Comparison of trajectories for different control strategies. —: Nonlinear programming solution. ·····: $f_{c,0}(t)$ given by Eq. (33). – – –: $f_{c,0}(t)$ given by Eq. (57).

Table 2
Absorbed mean power $\bar{P}$ [MW].

	Nonlinear programming	$f_{c,0}(t)$ given by Eq. (33)	$f_{c,0}(t)$ given by Eq. (57)
Realization 1	1.663	1.566 (5.8%)	1.544 (7.2%)
Realization 2	0.521	0.513 (1.2%)	0.467 (10.4%)
Realization 3	0.950	0.945 (0.5%)	0.921 (3.1%)

Values in brackets indicate the error relative to the nonlinear programming solution.

$$H_{r\dot{v}}(\omega) = \int_0^\infty e^{-i\omega t} h_{r\dot{v}}(t)\, dt \tag{6}$$

Combination of Eqs. (2), (4) and (5) provides the following integro-differential equation for $v(t)$ driven by $f_e(t)$ and $f_c(t)$ [21]:

$$\left.\begin{aligned} M\ddot{v}(t) + r(v(t)) + \int_{t_0}^{t} h_{r\dot{v}}(t-\tau)\dot{v}(\tau)\, d\tau = f_e(t) - f_c(t) \;\; t \in [t_0, t_1] \\ v(t_0) = v_0, \quad \dot{v}(t_0) = \dot{v}_0 \end{aligned}\right\} \tag{7}$$

where $M = m + m_h$, and v_0 and $\dot{v}_0$ are given initial conditions at the time t_0. t_1 is the terminal time of the control.

In Eq. (7), the term $r(v(t))$ represents a combined nonlinear restoring forces from the mooring system and from the buoyancy force due to noncylindrical outer shell of the absorber. In contrast, nonlinearities from the wave loading is ignored. The hydrodynamic nonlinearities originates from the dynamic Froude-Krylov force, the radiation force, the diffraction force and the viscous force. It turns out that the nonlinear radiation-diffraction force for heave point absorber is not significantly different from the one predicted by linear theory, and the viscous effects for heave point absorber seem to be negligible [23]. Hence, the hydrodynamic nonlinearities for heave point absorbers are mainly from the dynamic Froude-Krylov force [24]. It has been demonstrated that the numerical model with linear hydrodynamic coefficients is reasonably accurate for the point absorber oscillating in waves with a steepness factor $\frac{H_s}{\lambda_p} < 0.02$ [25], where H_s is the significant wave height, and λ_p the wavelength. In the numerical example below with $H_s = 3$ m and the peak period $T_p = 7.42$ s, this criterion is exceeded. Hence, the theory should be used merely as an approximation for such sea state.

Fig. 2 shows the impulse response function $h_{r\dot{v}}(t)$ based on the data indicated in Table 1 in the numerical example below. The time has

been normalized with respect to T_p. As seen, $h_{r\dot{v}}(t)$ effectively vanishes for $t > T_p$.

The wave excitation force $f_e(t)$ may be expressed in terms of the following convolution integral of the sea-surface elevation $\eta(t)$ [26]:

$$f_e(t) = \int_{-\infty}^{\infty} h_{e\eta}(t-\tau)\eta(\tau)d\tau \tag{8}$$

The sea-surface elevation $\eta(t)$ is assumed to be observed at a sufficient distant position from the absorber, where the measurement is not disturbed by the radiation wave, and $h_{e\eta}(t)$ is a non-causal impulse response function. The related frequency response function and the spectral density function become:

$$H_{e\eta}(\omega) = \int_{-\infty}^{\infty} e^{-i\omega t} h_{e\eta}(t)dt \tag{9}$$

$$S_{f_e f_e}(\omega) = |H_{e\eta}(\omega)|^2 S_{\eta\eta}(\omega) \tag{10}$$

The hydrodynamic parameters, i.e. k, m_h, $h_{r\dot{v}}(t)$, $H_{r\dot{v}}(\omega)$, $h_{e\eta}(t)$, $H_{e\eta}(\omega)$ can be calculated numerically. In the present case, the WAMIT program has been used, which is based on the boundary element method [27].

Fig. 3 shows the frequency response function $H_{r\dot{v}}(\omega)$. As follows from Eq. (6), $\mathrm{Re}(H_{r\dot{v}}(\omega)) = \int_0^{\infty} \cos(\omega t) h_{r\dot{v}}(t)\,dt$ and $\mathrm{Im}(H_{r\dot{v}}(\omega)) = \int_0^{\infty} \sin(\omega t) h_{r\dot{v}}(t)\,dt$. Since $h_{r\dot{v}}(t)$ is real, it follows that $\mathrm{Re}(H_{r\dot{v}}(\omega))$ is an even, and $\mathrm{Im}(H_{r\dot{v}}(\omega))$ an odd function of ω. For this reason, Fig. 3 only shows function values for $\omega > 0$.

In order to verify the theory by comparison to a numerical solution based on nonlinear programming, the convolution integral $f_{r,0}(t) = \int_{t_0}^{t} h_{r\dot{v}}(t-\tau)\dot{v}(\tau)\,d\tau$ needs to be replaced by a state vector approximation in terms of a system of linear, ordinary filter differential equations driven by the velocity $\dot{v}(t)$. The state vector formulation is based on an initial replacement of the actual frequency response function with an approximating rational function, leading to the following relations in the time domain:

$$\left.\begin{array}{c} f_{r,0}(t) = \mathbf{p}_r\,\mathbf{z}_r(t) \\ \frac{d}{dt}\mathbf{z}_r(t) = \mathbf{A}_r\,\mathbf{z}_r(t) + \mathbf{b}_r\,\dot{v}(t) \quad , t \in]t_0, t_1] \\ \mathbf{z}_r(t_0) = 0 \end{array}\right\} \tag{11}$$

The state vector $\mathbf{z}_r(t)$, the column vector $\mathbf{b}_r$, the system matrix $\mathbf{A}_r$ and the row vector $\mathbf{p}_r$ can be found in detail in Nielsen et al. [10]. Further, the initial value $\mathbf{z}_r(t_0) = \mathbf{0}$ follows because $f_{r,0}(t_0) = 0$.

According to the solution to the state vector differential equation in Eq. (11), $f_{r,0}(t)$ can be expressed as:

$$\begin{aligned} f_{r,0}(t) &= \int_{t_0}^{t} h_{r\dot{v}}(t-\tau)\,\dot{v}(\tau)\,d\tau \\ &= \int_{t_0}^{t} \boldsymbol{p}_r\, e^{\boldsymbol{A}_r(t-\tau)}\,\boldsymbol{b}_r\,\dot{v}(\tau)\,d\tau \end{aligned} \tag{12}$$

Hence, the impulse response function $h_{r\dot{v}}(t)$ is approximated as:

$$h_{r\dot{v}}(t) = \boldsymbol{p}_r\, e^{\boldsymbol{A}_r t}\,\boldsymbol{b}_r \tag{13}$$

Fig. 3 shows the obtained rational approximation of the order $(m, n) = (2, 3)$ to $H_{r\dot{v}}(\omega)$ compared with the target frequency response function.

Based on the double-sided auto-spectral density function $S_{f_e f_e}(\omega)$, a sufficient long time series of the wave load $f_e(t)$ may be generated. The time series in Fig. 4 was generated based on the JONSWAP spectrum defined in Eq. (54) below defined by H_s, T_p and the band-width parameter γ, using a rational linear filtration of a so-called broken line equivalent white noise process [28]. The wave load realization shown in Fig. 4 is used in subsequent numerical investigations.

The nonlinear algorithm indicated in the appendix will be used to validate the derived solution for the optimal constrained control force $f_c(t)$, which maximizes the absorbed power $P(t) = f_c(t)\,\dot{v}(t)$ in the interval $[t_0, t_1]$. The nonlinear algorithm depends on the accuracy of the state vector representation in Eq. (11) and on a discretization of the performance functional of the optimization problem. The rational approximation of the order $(m, n) = (2, 3)$ shown in Fig. 3 and a time step $\Delta t = \frac{1}{150}T_p$ will be applied. The validity of the nonlinear programming algorithm with the indicated rational approximation for the radiation force has been tested against the analytical solution for the unconstrained control force given as, [10]:

$$f_{c,0}(t) = -M\ddot{v}(t) - r(v(t)) + \int_{t}^{t_1} h_{r\dot{v}}(\tau - t)\dot{v}(\tau)\,d\tau \tag{14}$$

where the trajectories of $v(t)$, $\dot{v}(t)$, $\ddot{v}(t)$ are taken from the nonlinear programming solution.

Fig. 5 indicates the corresponding results. As seen, a perfect agreement is obtained both for the control force $f_{c,0}(t)$ and the instantaneous absorbed power $P_{opt,0}(t) = f_{c,0}(t)\,\dot{v}(t)$. For this reason, the nonlinear programming algorithm is considered appropriate also in the constrained optimization problem.

2.2. Optimal constrained control force

The displacement response $v(t)$ becomes large at optimal control because the control force $f_{c,0}(t)$ given by Eq. (14) tends to eliminate the nonlinear restoring force $r(v(t))$ and the inertial term $M\ddot{v}(t)$ in Eq. (7), making the system extremely flexible. However, only constraint on the control force caused by saturation of the actuator is considered in the following, given as:

$$f_{c,\min} \le f_c(t) \le f_{c,\max} \tag{15}$$

Maximizing the absorbed power during the control interval $]t_0, t_1]$ with constraints on the control force leads to the following control problem:

$$\left.\begin{array}{c} \max J[\dot{v}, f_c] = \int_{t_0}^{t_1} f_c(\tau)\dot{v}(\tau)\,d\tau \\ \text{subject to the path and control force constraints}: \\ \left\{\begin{array}{c} \dot{\boldsymbol{z}}(t) = \boldsymbol{g}(\boldsymbol{z}(t), f_c(t), t) \quad , t \in]t_0, t_1] \\ \boldsymbol{z}(t_0) = \boldsymbol{z}_0 \end{array}\right. \\ f_c(t) \in I_{f_c}, \quad t \in]t_0, t_1] \end{array}\right\} \tag{16}$$

where $I_{f_c} = [f_{c,\min}, f_{c,\max}]$ signifies the interval of admissible control forces. The state vector $\boldsymbol{z}(t)$ and the right-hand side of the state vector equation $\boldsymbol{g}(\boldsymbol{z}(t), f_c(t), t)$ are defined as:

$$\boldsymbol{z}(t) = \begin{bmatrix} v(t) \\ \dot{v}(t) \\ \boldsymbol{z}_r(t) \end{bmatrix} \tag{17}$$

$$\boldsymbol{g}(\boldsymbol{z}(t), f_c(t), t) = \begin{bmatrix} \dot{v}(t) \\ \frac{1}{M}\left(-\boldsymbol{p}_r\boldsymbol{z}_r(t) - r(v(t)) + f_e(t) - f_c(t)\right) \\ \boldsymbol{A}_r\boldsymbol{z}_r(t) + \boldsymbol{b}_r\dot{v}(t) \end{bmatrix} \tag{18}$$

The equivalent unconstrained optimization problem is given as:

$$\begin{aligned} \max \bar{J}[\boldsymbol{z}, \lambda, f_c] &= \int_{t_0}^{t_1} \left(f_c(\tau)\dot{v}(\tau) + \lambda^T(\tau)\left(\boldsymbol{g}(\boldsymbol{z}(\tau), f_c(\tau), \tau) - \dot{\boldsymbol{z}}(\tau)\right)\right) d\tau \\ &= \int_{t_0}^{t_1} \left(H(\mathbf{z}(\tau), \lambda(\tau), f_c(\tau), \tau) - \lambda^T(\tau)\,\dot{\boldsymbol{z}}(\tau)\right) d\tau \end{aligned} \tag{19}$$

where the Hamiltonian $H(\mathbf{z}(t), \lambda(t), f_c(t), t)$ of the control problem is

given as:

$$\begin{aligned}\mathrm{H}(\boldsymbol{z}(\mathrm{t}),\boldsymbol{\lambda}(\mathrm{t}),f_c(\mathrm{t}),\mathrm{t}) &= f_c(\mathrm{t})\,\dot{\mathrm{v}}(\mathrm{t}) + \boldsymbol{\lambda}^{\mathrm{T}}(\mathrm{t})\,\boldsymbol{g}(\boldsymbol{z}(\mathrm{t}),f_c(\mathrm{t}),\mathrm{t}) \\ &= -\frac{\lambda_{\dot{\mathrm{v}}}(\mathrm{t})}{\mathrm{M}}\,\mathrm{r}(\mathrm{v}(\mathrm{t})) + \left(f_c(\mathrm{t}) + \lambda_v(\mathrm{t}) + \boldsymbol{\lambda}_r^T(\mathrm{t})\,\boldsymbol{b}_{\mathrm{r}}\right)\,\dot{\mathrm{v}}(\mathrm{t}) \\ &+ \left(-\frac{\lambda_{\dot{\mathrm{v}}}(\mathrm{t})}{\mathrm{M}}\,\boldsymbol{p}_{\mathrm{r}} + \boldsymbol{\lambda}_r^T(\mathrm{t})\,\boldsymbol{A}_{\mathrm{r}}\right)\,\boldsymbol{z}_{\mathrm{r}}(\mathrm{t}) + \frac{\lambda_{\dot{\mathrm{v}}}(\mathrm{t})}{\mathrm{M}}\,\left(f_e(\mathrm{t}) - f_c(\mathrm{t})\right)\end{aligned} \tag{20}$$

and $\boldsymbol{\lambda}(t)$ is the co-state vector (Lagrange multiplier) defined as:

$$\boldsymbol{\lambda}(\mathrm{t}) = \begin{bmatrix}\lambda_v(\mathrm{t}) \\ \lambda_{\dot{\mathrm{v}}}(\mathrm{t}) \\ \boldsymbol{\lambda}_{\mathrm{r}}(\mathrm{t})\end{bmatrix} \tag{21}$$

Since there are no constraints on $\boldsymbol{z}(t)$ and $\boldsymbol{\lambda}(t)$, the first variation of Eq. (19) provides the following conditions for optimal control, valid for both constrained and unconstrained control forces:

$$\dot{\boldsymbol{z}}(\mathrm{t}) = \frac{\partial \mathrm{H}}{\partial \boldsymbol{\lambda}} = \boldsymbol{g}(\boldsymbol{z}(\mathrm{t}),f_c(\mathrm{t}),\mathrm{t}) \tag{22}$$

$$\dot{\boldsymbol{\lambda}}(\mathrm{t}) = -\frac{\partial \mathrm{H}}{\partial \boldsymbol{z}} \tag{23}$$

Eqs. (22) and (23) are known as the Hamiltonian equations (or canonical equations).

Conventionally, the trajectories of the state vector and the co-state vector at optimal control are denoted as $\boldsymbol{z}^*(t)$ and $\boldsymbol{\lambda}^*(t)$. Generally, the asterisks will be omitted in the following for ease of notation.

The terminal boundary condition (or transversality condition) on the co-state vector reads:

$$\boldsymbol{\lambda}(\mathrm{t}_1) = 0 \quad (\lambda_v(\mathrm{t}_1) = 0, \lambda_{\dot{\mathrm{v}}}(\mathrm{t}_1) = 0, \boldsymbol{\lambda}_{\mathrm{r}}(\mathrm{t}_1) = 0) \tag{24}$$

From Eqs. (20), (21) and (23) follows:

$$\begin{bmatrix}\dot{\lambda}_v(\mathrm{t}) \\ \dot{\lambda}_{\dot{\mathrm{v}}}(\mathrm{t}) \\ \dot{\boldsymbol{\lambda}}_{\mathrm{r}}(\mathrm{t})\end{bmatrix} = \begin{bmatrix}\frac{\partial \mathrm{r}(\mathrm{v}(\mathrm{t}))}{\partial \mathrm{v}}\frac{\lambda_{\dot{\mathrm{v}}}(\mathrm{t})}{\mathrm{M}} \\ -f_c(\mathrm{t}) - \lambda_v(\mathrm{t}) - \boldsymbol{b}_r^T\boldsymbol{\lambda}_{\mathrm{r}}(\mathrm{t}) \\ \boldsymbol{p}_r^T\frac{\lambda_{\dot{\mathrm{v}}}(\mathrm{t})}{\mathrm{M}} - \boldsymbol{A}_r^T\boldsymbol{\lambda}_{\mathrm{r}}(\mathrm{t})\end{bmatrix} \tag{25}$$

The 1st and 3rd equations in Eq. (25) in combination with the terminal conditions in Eq. (24) provide the following solutions for $\lambda_v(t)$ and $\boldsymbol{\lambda}_r(t)$:

$$\lambda_v(\mathrm{t}) = -\int_{\mathrm{t}}^{\mathrm{t}_1} \frac{\partial \mathrm{r}(\mathrm{v}(\tau))}{\partial \mathrm{v}}\frac{\lambda_{\dot{\mathrm{v}}}(\tau)}{\mathrm{M}}\,d\tau \tag{26}$$

$$\boldsymbol{\lambda}_{\mathrm{r}}(\mathrm{t}) = -\int_{\mathrm{t}}^{\mathrm{t}_1} \mathrm{e}^{\boldsymbol{A}_r^T(\tau-\mathrm{t})}\boldsymbol{p}_r^T\frac{\lambda_{\dot{\mathrm{v}}}(\tau)}{\mathrm{M}}\,d\tau \tag{27}$$

Insertion of Eqs. (26) and (27) into the second equation (25) results in the following expression for the optimal control force:

$$\begin{aligned}f_c(\mathrm{t}) &= -\dot{\lambda}_{\dot{\mathrm{v}}}(\mathrm{t}) + \boldsymbol{b}^{\mathrm{T}}\int_{\mathrm{t}}^{\mathrm{t}_1}\mathrm{e}^{\boldsymbol{A}_r^T(\tau-\mathrm{t})}\boldsymbol{p}_r^T\frac{\lambda_{\dot{\mathrm{v}}}(\tau)}{\mathrm{M}}\,d\tau - \int_{\mathrm{t}}^{\mathrm{t}_1}\frac{\partial \mathrm{r}(\mathrm{v}(\tau))}{\partial \mathrm{v}}\frac{\lambda_{\dot{\mathrm{v}}}(\tau)}{\mathrm{M}}\,d\tau \\ &= -\dot{\lambda}_{\dot{\mathrm{v}}}(\mathrm{t}) + \int_{\mathrm{t}}^{\mathrm{t}_1}\mathrm{h}_{\mathrm{r}\dot{\mathrm{v}}}(\tau-\mathrm{t})\frac{\lambda_{\dot{\mathrm{v}}}(\tau)}{\mathrm{M}}\,d\tau - \int_{\mathrm{t}}^{\mathrm{t}_1}\frac{\partial \mathrm{r}(\mathrm{v}(\tau))}{\partial \mathrm{v}}\frac{\lambda_{\dot{\mathrm{v}}}(\tau)}{\mathrm{M}}\,d\tau\end{aligned} \tag{28}$$

In the last statement it has been used that $\boldsymbol{b}_r^T\mathrm{e}^{\boldsymbol{A}_r^T\mathrm{t}}\boldsymbol{p}_r^T = \boldsymbol{p}_{\mathrm{r}}\,\mathrm{e}^{\boldsymbol{A}_{\mathrm{r}}\mathrm{t}}\boldsymbol{b}_{\mathrm{r}} = \mathrm{h}_{\mathrm{r}\dot{\mathrm{v}}}(\mathrm{t})$, cf. Eq. (13). Eq. (28) holds for both constrained and unconstrained control forces.

The optimal control for constrained control force follows from the Pontryagin maximum principle, [29]:

$$\mathrm{H}(\boldsymbol{z}^*(\mathrm{t}),\boldsymbol{\lambda}^*(\mathrm{t}),f_c^*(\mathrm{t}),\mathrm{t}) = \max_{f_c(\mathrm{t})\in\mathrm{I}_{f_c}}\mathrm{H}(\boldsymbol{z}^*(\mathrm{t}),\boldsymbol{\lambda}^*(\mathrm{t}),f_c(\mathrm{t}),\mathrm{t}) \tag{29}$$

Based on first order variations, Eqs. (22), (23) and (29) are merely necessary conditions for optimality.

Since the Hamiltonian given by Eq. (20) is linear in the control force $f_c(t)$ with the proportionality factor $\dot{\mathrm{v}}(\mathrm{t}) - \frac{\lambda_{\dot{\mathrm{v}}}(\mathrm{t})}{\mathrm{M}}$, Eq. (29) provides the following solution for the optimal control force:

$$f_c(\mathrm{t}) = \begin{cases}\mathrm{f}_{\mathrm{c,max}}, & \lambda_{\dot{\mathrm{v}}}(\mathrm{t}) < \mathrm{M}\dot{\mathrm{v}}(\mathrm{t}) \\ \mathrm{f}_{\mathrm{c},0}(\mathrm{t}), & \lambda_{\dot{\mathrm{v}}}(\mathrm{t}) = \mathrm{M}\dot{\mathrm{v}}(\mathrm{t}) \\ \mathrm{f}_{\mathrm{c,min}}, & \lambda_{\dot{\mathrm{v}}}(\mathrm{t}) > \mathrm{M}\dot{\mathrm{v}}(\mathrm{t})\end{cases} \tag{30}$$

The undetermined quantity $f_{c,0}(t)$ is related to the condition:

$$\lambda_{\dot{\mathrm{v}}}(\mathrm{t}) = \mathrm{M}\dot{\mathrm{v}}(\mathrm{t}) \tag{31}$$

Under the condition in Eq. (31) follows:

$$\frac{\partial \mathrm{r}(\mathrm{v}(\mathrm{t}))}{\partial \mathrm{v}}\frac{\lambda_{\dot{\mathrm{v}}}(\mathrm{t})}{\mathrm{M}} = \frac{\partial \mathrm{r}(\mathrm{v}(\mathrm{t}))}{\partial \mathrm{v}}\dot{\mathrm{v}}(\mathrm{t}) = \frac{\mathrm{dr}(\mathrm{v}(\mathrm{t}))}{\mathrm{dt}} \tag{32}$$

Then, $f_{c,0}(t)$ is obtained by insertion of Eqs. (31) and (32) in Eq. (28):

$$\begin{aligned}\mathrm{f}_{\mathrm{c},0}(\mathrm{t}) = &-\mathrm{M}\ddot{\mathrm{v}}(\mathrm{t}) + \int_{\mathrm{t}}^{\mathrm{t}_1}\mathrm{h}_{\mathrm{r}\dot{\mathrm{v}}}(\tau-\mathrm{t})\dot{\mathrm{v}}(\tau)d\tau \\ &- \mathrm{r}(\mathrm{v}(\mathrm{t})) + \mathrm{r}(\mathrm{v}(\mathrm{t}_1))\end{aligned} \tag{33}$$

The term $\mathrm{r}(\mathrm{v}(\mathrm{t}_1))$ indicates a static control force components, which may be used to counteract a static restoring force component corresponding to the static drift $\mathrm{v}(\mathrm{t}_1)$ of the absorber. Since, the displacement of the absorber is referred to the static equilibrium state, no static offset is present, and so the said term may be set to zero. Hence, Eq. (33) reduces to Eq. (14), which was originally obtained based on the unconstrained first order variation of the performance functional in Eq. (19). This leads to the control law equation $\frac{\partial \mathrm{H}}{\partial f_c} = 0$, resulting again in Eq. (31).

$f_{c,0}(t)$ may attain arbitrary large positive and negative values. Then, the condition $\lambda_{\dot{\mathrm{v}}}(\mathrm{t}) < \mathrm{M}\dot{\mathrm{v}}(\mathrm{t})$ specifies values, where $f_{c,0}(t) > f_{c,\max}$, and the condition $\lambda_{\dot{\mathrm{v}}}(\mathrm{t}) > \mathrm{M}\dot{\mathrm{v}}(\mathrm{t})$ correspondingly values fulfilling $f_{c,0}(t) < f_{c,\min}$. Hence, $f_{c,0}(t)$ may be used as a saturation parameter. Then, the final form of the constrained optimal control law may be written as:

$$f_c(\mathrm{t}) = \begin{cases}\mathrm{f}_{\mathrm{c,max}}, & \mathrm{f}_{\mathrm{c},0}(\mathrm{t}) > \mathrm{f}_{\mathrm{c,max}} \\ \mathrm{f}_{\mathrm{c},0}(\mathrm{t}) & \\ \mathrm{f}_{\mathrm{c,min}}, & \mathrm{f}_{\mathrm{c},0}(\mathrm{t}) < \mathrm{f}_{\mathrm{c,min}}\end{cases} \tag{34}$$

Eq. (34) specifies a non-causal control law at the time t with feedback from the present displacement $\mathrm{v}(t)$ and acceleration $\ddot{\mathrm{v}}(t)$, and feedback from future velocities $\dot{\mathrm{v}}(\tau), \tau \in]\mathrm{t}, \mathrm{t}_1]$. Hence, a prediction algorithm of future velocities $\dot{\mathrm{v}}(\tau), \tau \in]\mathrm{t}, \mathrm{t}_1]$ is needed at practical applications, which will be dealt with in a later section. Due to the inherent uncertainty related to the prediction procedure, the resulting controller will merely be sub-optimal.

In order to verify Eq. (34), the optimal trajectories of $\mathrm{v}(t)$, $\dot{\mathrm{v}}(t)$ and $\ddot{\mathrm{v}}(t)$ obtained from nonlinear programming are inserted in Eq. (34), and the resulting control force and resulting instantaneous absorbed power are compared to the corresponding solutions obtained directly by nonlinear programming. Fig. 6 shows the results for a control force constraint $f_{c,\max} = -f_{c,\min} = 2 \times 10^6\,\mathrm{N}$ and unconstrained displacement. As seen, by comparison of Fig. 6a and b with Fig. 5a and b, the optimal displacement and velocity trajectories are only slightly affected by the control force constraint. Fig. 6c and d show the results for the optimal control force given by Eq. (34) and instantaneous absorbed power, in comparison to the corresponding nonlinear programming solution. As seen, no disagreement is visible.

2.3. Prediction of future velocity

In order to predict the future velocity response $\dot{\mathrm{v}}(\mathrm{t}), \mathrm{t} > \mathrm{t}_0$, a van der Pol transformation of the narrow-banded processes $\dot{\mathrm{v}}(t)$ and $\ddot{\mathrm{v}}(t)$ is intro-

duced, given as [18]:

$$\left.\begin{array}{l} \dot{v}(t) = a(t)\cos(\omega_p t + \varphi(t)) \\ \ddot{v}(t) = -\omega_p a(t)\sin(\omega_p t + \varphi(t)) \end{array}\right\} \tag{35}$$

where $a(t)$ and $\varphi(t)$ signify slowly varying amplitude and phase processes, expressed as:

$$\left.\begin{array}{l} a(t) = \sqrt{\dot{v}^2(t) + \left(\frac{\ddot{v}(t)}{\omega_p}\right)^2} \\ \varphi(t) = \arctan\left(-\frac{\ddot{v}(t)}{\omega_p \dot{v}(t)}\right) - \omega_p t \end{array}\right\} \tag{36}$$

Fig. 7 shows realizations of $a(t)$ and $\varphi(t)$ for the constrained absorber. As seen, the evolution of $a(t)$ and $\varphi(t)$ take place over several periods. Because $h_{r\dot{v}}(t) \simeq 0$ for $t > T_p$ as shown in Fig. 2, a prediction of $a(t)$, $\varphi(t)$ and hence $\dot{v}(t)$ is only needed one peak wave period T_p ahead of the present time t_0.

Defined the following quantities:

$$\left.\begin{array}{l} a_{-j} = a(t_0 - jT_p) \\ \varphi_{-j} = \varphi(t_0 - jT_p) \end{array}\right\}, \quad j = 0, 1, 2, \ldots \tag{37}$$

Then, the predicted velocities can be formulated as:

$$\dot{v}(t) = a(t)\cos(\omega_p t + \varphi(t)), \quad t > t_0 \tag{38}$$

$a(t)$ and $\varphi(t)$ are estimated by extrapolation from $t = t_0$ of 2nd order Lagrange polynomials calibrated through the function values at t_0, $t_0 - T_p$ and $t - 2T_p$, given as:

$$\left.\begin{array}{l} a(t) = a_0 + \frac{1}{2}(3a_0 - 4a_{-1} + a_{-2})\tau + \frac{1}{2}(a_0 - 2a_{-1} + a_{-2})\tau^2 \\ \varphi(t) = \varphi_0 + \frac{1}{2}(3\varphi_0 - 4\varphi_{-1} + \varphi_{-2})\tau + \frac{1}{2}(\varphi_0 - 2\varphi_{-1} + \varphi_{-2})\tau^2 \end{array}\right\}, \quad \tau = \frac{t - t_0}{Tp} \geq 0 \tag{39}$$

Fig. 8 shows the prediction of $\dot{v}(t)$ from $t = 14.25T_p$, $t = 15.25T_p$ and $t = 16.25T_p$. As seen, the predicted velocities fit well at least one period ahead, which is the required prediction horizon with the impulse response function shown in Fig. 2.

Alternatively, $a(t)$ and $\varphi(t)$ may be estimated by using the Hilbert transformation $\hat{\dot{v}}(t)$ of the velocity response instead of $\frac{\ddot{v}(t)}{\omega_p}$ in Eq. (36) [30,31]. The two approaches are identical for harmonic varying functions $\dot{v}(t)$ and $\ddot{v}(t)$.

2.4. Mean absorbed power at optimal control

In the following, the restoring force from buoyancy and mooring is assumed to be linear, i.e. $r(v(t)) = k\,v(t)$.

At optimal unconstrained control, the frequency response function $H_{\dot{v}f_e}(\omega)$ for the velocity response $\dot{v}(t)$ due to the harmonic varying wave load $f_e(t)$ is given as, [26]:

$$H_{\dot{v}f_e}(\omega) = \frac{1}{2\,\mathrm{Re}(H_{r\dot{v}}(\omega))} \tag{40}$$

Then, the double-sided auto-spectral density function $S_{\dot{v}\dot{v}}(\omega)$ of the related velocity response process becomes, [28]

$$\begin{aligned} S_{\dot{v}\dot{v}}(\omega) &= |H_{\dot{v}f_e}(\omega)|^2 S_{f_e f_e}(\omega) \\ &= \frac{|H_{e\eta}(\omega)|^2}{4\left(\mathrm{Re}(H_{r\dot{v}}(\omega))\right)^2} S_{\eta\eta}(\omega) \end{aligned} \tag{41}$$

where Eq. (10) has been used in the last statement.

Due to the linear relationship between $\dot{v}(t)$ and $f_e(t)$ as reflected by Eq. (40), $\dot{v}(t)$ becomes Gaussian, if the wave load process is Gaussian. Then, the acceleration process $\ddot{v}(t)$ and the displacement process $v(t)$ become Gaussian processes as well.

In turn, $f_{c,0}(t)$ as given by Eq. (14) becomes Gaussian, if the restoring force is linear.

The auto-spectral density function $S_{f_{c,0}f_{c,0}}(\omega)$ of $f_{c,0}(t)$ and the cross-spectral density function $S_{f_{c,0}\dot{v}}(\omega)$ of $f_{c,0}(t)$ and $\dot{v}(t)$ become, [28]:

$$\left.\begin{array}{rcl} S_{f_{c,0}f_{c,0}}(\omega) & = & |H_{f_{c,0}\dot{v}}(\omega)|^2 S_{\dot{v}\dot{v}}(\omega) \\ & = & \left(\left(\omega M - \frac{k}{\omega} - \mathrm{Im}(H_{r\dot{v}}(\omega))\right)^2 + \left(\mathrm{Re}(H_{r\dot{v}}(\omega))\right)^2\right) S_{\dot{v}\dot{v}}(\omega) \\ S_{f_{c,0}\dot{v}}(\omega) & = & H^*_{f_{c,0}\dot{v}}(\omega)\, S_{\dot{v}\dot{v}}(\omega) = \left(i\omega M + H^*_{r\dot{v}}(\omega) + \frac{k}{i\omega}\right) S_{\dot{v}\dot{v}}(\omega) \end{array}\right\} \tag{42}$$

where $H^*_{f_{c,0}\dot{v}}(\omega)$ and $H^*_{r\dot{v}}(\omega)$ signify the complex conjugate of $H_{f_{c,0}\dot{v}}(\omega)$ and $H_{r\dot{v}}(\omega)$. $H_{f_{c,0}\dot{v}}(\omega)$ is given as:

$$H_{f_{c,0}\dot{v}}(\omega) = -i\omega M + H_{r\dot{v}}(\omega) - \frac{k}{i\omega} \tag{43}$$

The variances $\sigma^2_{\dot{v}}$ and $\sigma^2_{f_{c,0}}$ and the covariance $\kappa_{f_{c,0}\dot{v}}$ of $f_{c,0}(t)$ and $\dot{v}(t)$ follow from Eqs. (41) and (42), [28]:

$$\left.\begin{array}{rcl} \sigma^2_{\dot{v}} & = & \int_{-\infty}^{\infty} S_{\dot{v}\dot{v}}(\omega)d\omega = \int_0^{\infty} \frac{|H_{e\eta}(\omega)|^2}{2(\mathrm{Re}(H_{r\dot{v}}(\omega)))^2} S_{\eta\eta}(\omega)\, d\omega \\ \sigma^2_{f_{c,0}} & = & \int_{-\infty}^{\infty} |H_{f_{c,0}\dot{v}}(\omega)|^2\, S_{\dot{v}\dot{v}}(\omega)\, d\omega \\ & = & 2\int_0^{\infty} \left(\left(\omega M - \frac{k}{\omega} - \mathrm{Im}(H_{r\dot{v}}(\omega))\right)^2 + \left(\mathrm{Re}(H_{r\dot{v}}(\omega))\right)^2\right) S_{\dot{v}\dot{v}}(\omega)\, d\omega \\ \kappa_{f_{c,0}\dot{v}} & = & \int_{-\infty}^{\infty} H^*_{f_{c,0}\dot{v}}(\omega)\, S_{\dot{v}\dot{v}}(\omega)\, d\omega = 2\int_0^{\infty} \mathrm{Re}(H_{r\dot{v}}(\omega))\, S_{\dot{v}\dot{v}}(\omega)\, d\omega \end{array}\right\}$$

The final results in Eq. (44) follow, because the real and imaginary parts of the involved frequency response functions are odd and even function of ω, respectively, and $S_{\dot{v}\dot{v}}(\omega)$ is an even function of ω. The quadratures in Eq. (44) need to be evaluated numerically.

The maximum mean power that can be extracted by the unconstrained optimal control from an irregular sea state is expressed as, Nielsen et al. [10]:

$$\bar{P}_{opt,0} = \int_0^{\infty} \frac{|H_{e\eta}(\omega)|^2}{2\,\mathrm{Re}(H_{r\dot{v}}(\omega))} S_{\eta\eta}(\omega)\, d\omega \tag{45}$$

The joint probability density function $p_{f_{c,0}\dot{v}}(f, \dot{v})$ of $f_{c,0}(t)$ and $\dot{v}(t)$ is bi-variate normal distributed with the statistical moments given in Eq. (44). $p_{f_{c,0}\dot{v}}(f, \dot{v})$ may be written on the form:

$$p_{f_{c,0}\dot{v}}(f, \dot{v}) = \frac{1}{\sigma_{f_{c,0}}} \varphi\left(\frac{f}{\sigma_{f_{c,0}}}\right) \frac{1}{\sigma} \varphi\left(\frac{\dot{v} - \mu(f)}{\sigma}\right) \tag{46}$$

$\varphi(\cdot)$ indicates the standardized normal probability density function, $\mu(f)$ and σ signifies the mean value and standard deviation of $\dot{v}(t)$ on condition of the sample $f_{c,0}(t) = f$, given as:

$$\left.\begin{array}{rcl} \mu(f) & = & \rho\frac{\sigma_{\dot{v}}}{\sigma_{f_{c,0}}} f \\ \sigma & = & \sqrt{1 - \rho^2}\sigma_{\dot{v}} \end{array}\right\} \tag{47}$$

ρ is the correlation coefficient of $\dot{v}(t)$ and $f_{c,0}(t)$ given as:

$$\rho = \frac{\kappa_{f_{c,0}\dot{v}}}{\sigma_{f_{c,0}}\sigma_{\dot{v}}} \tag{48}$$

Next, the maximal mean power absorbed by the constrained control force $f_c(t)$ given by Eq. (34) may be calculated from the following linear combination of conditional expectations:

$$\begin{aligned}\bar{P}_{opt} &= E[f_c(t)\dot{v}(t)] \\ &= E[f_c(t)\dot{v}(t)\,|\,f_c(t) = f_{c,max}]\,P(f_{c,0}(t)>f_{c,max}) \\ &\quad + E[f_c(t)\dot{v}(t)\,|\,f_{c,min} \le f_c(t) \le f_{c,max}]\,P(f_{c,min} \le f_{c,0}(t) \le f_{c,max}) \\ &\quad + E[f_c(t)\dot{v}(t)\,|\,f_c(t) = f_{c,min}]\,P(f_{c,0}(t)<f_{c,min})\end{aligned} \tag{49}$$

where:

$$\left.\begin{aligned} P(f_{c,0}(t)>f_{c,max}) &= 1-\Phi\left(\frac{f_{c,max}}{\sigma_{f_{c,0}}}\right) \\ P(f_{c,min} \le f_{c,0}(t) \le f_{c,max}) &= \Phi\left(\frac{f_{c,max}}{\sigma_{f_{c,0}}}\right)-\Phi\left(\frac{f_{c,min}}{\sigma_{f_{c,0}}}\right) \\ P(f_{c,0}(t)<f_{c,min}) &= \Phi\left(\frac{f_{c,min}}{\sigma_{f_{c,0}}}\right)\end{aligned}\right\} \tag{50}$$

$$\begin{aligned} E[f_c(t)\dot{v}(t)\,|\,f_c(t) &= f_{c,max}] = f_{c,max}\,E[\dot{v}(t \\ &= f_{c,max}\,\mu(f_{c,max}) = (\\ E[f_c(t)\dot{v}(t)\,|\,f_{c,min} \le f_c(t) \le f_{c,max}] &= \int_{f_{c,min}}^{f_{c,max}} f \int_{-\infty}^{\infty} \dot{v}\,p_{f} \\ &= \int_{f_{c,min}}^{f_{c,max}} f\,\mu(f)\,\frac{1}{\sigma_{f_{c,0}}} \\ &= \left(\Phi\left(\frac{f_{c,max}}{\sigma_{f_{c,0}}}\right)-\Phi\left(\frac{f_{c,min}}{\sigma_{f_{c,0}}}\right)-\frac{f_{c,max}}{\sigma_{f_{c,0}}}\varphi\left(\right.\right. \\ E[f_c(t)\dot{v}(t)|f_c(t) = f_{c,min}] &= f_{c,min}E[\dot{v}(t)|f_{c,0} \\ &= f_{c,min}\,\mu(f_{c,min}) = (\end{aligned}$$

where $\Phi(\cdot)$ indicates the standardized normal probability distribution function.

Insertion of the results in Eqs. (50) and (51) in Eq. (49) provides the following solution for the maximal mean power that can be absorbed by the constrained control force:

$$\bar{P}_{opt} = \alpha(f_{c,min}, f_{c,max})\bar{P}_{opt,0} \tag{52}$$

where $\alpha(f_{c,min}, f_{c,max})$ is a reduction factor caused by the constraints on the control force:

$$\begin{aligned}\alpha(f_{c,min}, f_{c,max}) = &\left(\Phi\left(\frac{f_{c,max}}{\sigma_{f_{c,0}}}\right)-\Phi\left(\frac{f_{c,min}}{\sigma_{f_{c,0}}}\right)\right)^2 \\ &-\left(\frac{f_{c,max}}{\sigma_{f_{c,0}}}\varphi\left(\frac{f_{c,max}}{\sigma_{f_{c,0}}}\right)-\frac{f_{c,min}}{\sigma_{f_{c,0}}}\varphi\left(\frac{f_{c,min}}{\sigma_{f_{c,0}}}\right)\right)\left(\Phi\left(\frac{f_{c,max}}{\sigma_{f_{c,0}}}\right)-\Phi\right. \\ &+\left(\frac{f_{c,max}}{\sigma_{f_{c,0}}}\right)^2\left(1-\Phi\left(\frac{f_{c,max}}{\sigma_{f_{c,0}}}\right)\right)+\left(\frac{f_{c,min}}{\sigma_{f_{c,0}}}\right)^2\Phi\left(\frac{f_{c,n}}{\sigma_{f_c}}\right.\end{aligned}$$

Fig. 9 shows the variation of $\alpha(f_{c,min}, f_{c,max})$ as a function of $\frac{f_{c,max}}{\sigma_{f_{c,0}}}$, $f_{c,min} = -f_{c,max}$. As seen, the constraints are only active for $\min(f_{c,max}, -f_{c,min}) < 3\sigma_{f_{c,0}}$.

3. Numerical example

A point heave wave energy converter indicated in Fig. 1 is considered in the numerical simulation. Table 1 indicates the relevant data of the absorber and the wave excitation parameters and the optimized gain parameters in Eq. (57).

$S_{\eta\eta}(\omega)$ is taken as the double-sided JONSWAP auto spectral density function given as [32]:

$$S_{\eta\eta}(\omega) = \delta\frac{H_s^2}{\omega_p}\gamma^{\beta}\left(\frac{|\omega|}{\omega_p}\right)^{-5}\exp\left(-\frac{5}{4}\left(\frac{\omega}{\omega_p}\right)^{-4}\right) \tag{54}$$

where

$$\left.\begin{aligned}\delta &= \frac{0.0312}{0.230+0.0336\gamma-\frac{0.185}{1.9+\gamma}} \\ \beta &= \exp\left(-\frac{1}{2}\left(\frac{|\omega|-\omega_p}{\sigma\omega_p}\right)^2\right) \\ \sigma &= \begin{cases}0.07, & |\omega| \le \omega_p \\ 0.09, & |\omega| > \omega_p\end{cases}\end{aligned}\right\} \tag{55}$$

T_p is the peak period, $\omega_p = \frac{2\pi}{T_p}$ is the related angular peak frequency and H_s is the significant wave height. γ is the so-called peak enhancement parameter which controls the bandwidth of the spectrum.

It is well known that the optimal control of point absorber in monochromatic waves is achieved when the control force enforces the absorber into resonance with the harmonic varying wave force. In this respect, the value of $k = 1.51 \times 10^5$ N/m has been chosen in the numerical analysis below, corresponding to the undamped angular eigenfrequency $\omega_0 = 0.81$ rad/s, which is close to the peak angular eigenfrequency $\omega_p = 0.85$ rad/s, in order to reduce the control effort even in irregular sea states.

In applications, $\ddot{v}(t)$ may be measured by an accelerometer, from which $v(t)$ and $\dot{v}(t)$ are obtained by numerical integration. However, $\ddot{v}(t)$ may be corrupted by measurement noise. In order to analyze the influence of the noise on the quality of the control, $\ddot{v}(t)$ is written in the form:

$$\ddot{v}(t) = \ddot{v}_0(t) + a_1 w(t) \tag{56}$$

where $\ddot{v}_0(t)$ is the acceleration predicted by nonlinear programming. The parameter a_1 indicates the level of noise, and $w(t)$ signifies a zero mean, stationary, broadbanded Gaussian stochastic process with an auto spectral density function, which is flat at the value $\frac{1}{2\pi}$ in the angular frequency interval $[0, 2\omega_p]$, mimicking a unit intensity Gaussian white noise [28]. Fig. 10 shows the obtained control forces with different noise levels $a_1 = 0.5\ m/s^{1/2}$, $a_1 = 0.05\ m/s^{1/2}$ and $a_1 = 0.001\ m/s^{1/2}$.

As seen, the obtained control force is sensible to observation noise when $a_1 \ge 0.05\ m/s^{1/2}$. The reason is that the inertial term is dominating in the solution Eq. (34), and the noise in the acceleration signal is amplified by multiplication with M.

The quality of the estimated control force will influence the future response. The extent of this will next be investigated. The detail of the procedure can be expressed as:

(1) At the time t, predict $\dot{v}(\tau)$ for τ in the interval $[t, t + T_p]$.
(2) Calculate $f_{c,0}(t)$ and $f_c(t)$ from Eqs. (33) and (34).
(3) Integrate Eq. (7) one time step Δt ahead to obtain $v(t + \Delta t)$, $\dot{v}(t + \Delta t)$ and $\ddot{v}(t + \Delta t)$, keeping $f_c(t)$ constant in the interval $[t, t + \Delta t]$.
(4) Update $f_c(t)$.

The procedure mimics the practical application of the control, where the control force needs to be applied as a piecewise constant function.

Additionally, comparison will be made with the following causal unconstrained control force in Eq. (34):

$$f_{c,0}(t) = -\beta_1 M\ddot{v}(t) + c\dot{v}(t) - \beta_2 r(v(t)) \tag{57}$$

Eq. (57) can be characterized as a controller with feedback from the displacement, velocity and the present acceleration. The first and the third terms introduce negative inertia and stiffness into the system. Guided by the theoretical solution in Eq. (33), these parameters should be close to one. The viscous damping term replaces the radiation damping term in Eq. (33). Obviously, the gain parameters β_1, β_2, c depend on the considered sea-state.

Figs. 11–13 indicate the performance of the suggested control law compared to those obtained by nonlinear programming and the feed-

back control in Eq. (57) for three independent realizations of the surface elevation of a sea-state defined by $H_s = 3$ m, $T_p = 7.42$ s, $\gamma = 5$. The control interval is chosen as $[t_0, t_1] = [0, 20T_p]$, and the same optimized parameters β_1, β_2, c as indicated in Table 1 are used for three realizations. The related absorbed mean power have been indicated in Table 2.

As seen from Figs. 11, 12 and 13, the displacement and velocity estimates based on the two approximate control related to Eqs. (34) and (57) are not deviating much from the nonlinear programming solution. However, the control force and the instantaneous power takeoff deviate substantially. Again, this is because the deviations in the related acceleration signals are amplified significantly when multiplied by M.

Table 2 compares the mean absorbed power $\bar{P}$ in the indicated interval $[3.5T_p, 20T_p]$ for the considered control strategy with the solutions from nonlinear programming and the optimized causal control with $f_{c,0}(t)$ given by Eq. (57).

As seen, the absorbed mean power by the control laws is less deviating than the instantaneous power takeoff. As shown in Table 2, the absorbed mean power for the control law with $f_{c,0}(t)$ given by Eq. (33) and with predicted future velocities are between 0.5% and 5.8% lower than the nonlinear programming solution for the optimal control. Further, the mean power takeoff for the control law with $f_{c,0}(t)$ given by Eq. (57) is further reduced compared to the suggested control law.

4. Conclusions

This paper presents an analytical solution for the optimal power take-off of a heave point wave energy converter with the constrained control force. Based on the solution for the optimal control force, the mean absorbed power take-off in a given sea-state has been derived. The optimal control force has a noncausal dependence on future velocities, which need to be predicted. The response processes turn out to be narrow-banded with the peak angular frequency as center frequency. This observation is used in the prediction algorithm, which is based on a van der Pol transformation of velocity and acceleration of the absorber. The mean power takeoff of the suggested control law, applied in a way mimicking the application in reality, was compared to that of optimal control obtained by nonlinear programming for three independent realizations of a given sea-state. The reduction in efficiency varied between 0.5% and 5.8%. Finally, the controller was compared to a causal controller with feedback from the present displacement, velocity and acceleration, which turn out to perform worse in all three cases.

Acknowledgements

The authors gratefully acknowledge the financial support from project 675659-ICONN-H2020-MSCA-ITN-2015.

Appendix A. Nonlinear programming algorithm

The optimal control problem in Eq. (16) is reformulated as a nonlinear programming problem by discretizing the objective functional and the state vector in time:

$$\max\ \mathrm{J}(\mathbf{X}(\tau_M)) = \mathrm{x}_{n+3}(\tau_M)$$

subject to the path and inequality constraints :

$$\mathbf{h}(\mathbf{X}(\tau_j)) = \left.\begin{bmatrix} \mathbf{c}(\mathbf{X}(\tau_j)) = 0 \\ \begin{bmatrix} \mathrm{v}(\tau_j) - \mathrm{v}_{\max} \\ -\mathrm{v}(\tau_j) + \mathrm{v}_{\min} \\ f_c(\tau_j) - \mathrm{f}_{\mathrm{c,max}} \\ -f_c(\tau_j) + \mathrm{f}_{\mathrm{c,min}} \end{bmatrix} - \mathbf{s}(\tau_j) = 0 \\ \mathbf{s}(\tau_j) \geq 0 \end{bmatrix}\right\} \tag{58}$$

where $\tau_j = t_0 + j\Delta\tau\ j = 0, 1, \ldots, M$.

$\mathbf{s}(t)$ indicates a vector function of slack variables. The time step in the discretization of the interval $]t_0, t_1]$ is given as $\Delta\tau = \frac{t_1 - t_0}{M}$. The vector $\mathbf{X}(t)$ of dimension $2n + 6$ and the path constrain vector $\mathbf{c}(\mathbf{X}(t))$ of dimension $n + 3$ are defined as:

$$\mathbf{X}(\mathrm{t}) = \left[\mathrm{v}(\mathrm{t}), \dot{\mathrm{v}}(\mathrm{t}), \mathbf{z}_r^T(\mathrm{t}), \mathrm{x}_{n+3}(\mathrm{t}), \frac{d}{\mathrm{dt}}\mathrm{v}(\mathrm{t}), \frac{d}{\mathrm{dt}}\dot{\mathrm{v}}(\mathrm{t}), \frac{d}{\mathrm{dt}}\mathbf{z}_r^T(\mathrm{t}), \frac{d}{\mathrm{dt}}\mathrm{x}_{n+3}(\mathrm{t})\right]^{\mathrm{T}} \tag{59}$$

$$\mathbf{c}(\mathbf{X}(\mathrm{t})) = \begin{bmatrix} \frac{d}{\mathrm{dt}}\mathrm{v}(\mathrm{t}) - \dot{\mathrm{v}}(\mathrm{t}) \\ \mathrm{M}\frac{d}{\mathrm{dt}}\dot{\mathrm{v}}(\mathrm{t}) + \mathbf{p}_{\mathrm{r}}\mathbf{z}_{\mathrm{r}}(\mathrm{t}) + \mathrm{r}(\mathrm{v}(\mathrm{t})) - f_e(\mathrm{t}) + f_c(\mathrm{t}) \\ \frac{d}{\mathrm{dt}}\mathbf{z}_{\mathrm{r}}(\mathrm{t}) - \mathbf{A}_{\mathrm{r}}\,\mathbf{z}_{\mathrm{r}}(\mathrm{t}) - \mathbf{b}_{\mathrm{r}}\,\dot{\mathrm{v}}(\mathrm{t}) \\ \frac{d}{\mathrm{dt}}\mathrm{x}_{n+3}(\mathrm{t}) - f_c(\mathrm{t})\dot{\mathrm{v}}(\mathrm{t}) \end{bmatrix} \tag{60}$$

The inherent approximation in the indicated nonlinear programming formulation concerns the discretization of the time continuous problem into $M + 1$ discrete instants of time for optimization, and the use of the rational approximation in Eq. (13) for the force $f_{r,0}(t)$.

The formulation applies to both displacement constraints and control force constraints. In case, merely control force constraints are prescribed the algorithm is applied by using large values of $v_{\max}$ and small values of $v_{\min}$.

The applied algorithm for solving the indicated nonlinear programming problem is described in [33].

References

[1] J.V. Ringwood, G. Bacelli, F. Fusco, Energy-maximizing control of wave-energy converters: the development of control system technology to optimize their operation, IEEE Control Syst. 34 (5) (2014) 30–55.
[2] J. Falnes, Wave-power conversion by point absorber, Nor. Marit. Res. 6 (4) (1978).
[3] M.J. French, A generalized view of resonant energy transfer, J. Mech. Eng. Sci. 21 (4) (1979) 299–300.
[4] R.E. Hoskin, N.K. Nichols, Latching Control for the Point-absorber Wave-power Device, University of Reading. Department of Mathematics, 1986.
[5] U.A. Korde, Latching control of deep water wave energy devices using an active reference, Ocean Eng. 29 (11) (2002) 1343–1355.
[6] A. Babarit, A.H. Clement, Optimal latching control of a wave energy device in regular and irregular waves, Appl. Ocean Res. 28 (2) (2006) 77–91.
[7] A. Babarit, M. Guglielmi, A.H. Clement, Declutching control of a wave energy converter, Ocean Eng. 36 (12-13) (2009) 1015–1024.
[8] K.J. Åström, T. Hägglund, Advanced PID Control, ISA – The Instrumentation, Systems and Automation Society, 2006.
[9] S. Peretta, P. Ruol, L. Martinelli, A. Tetu, J.P. Kofoed, Effect of a negative stiffness mechanism on the performance of the WEPTOS rotors, In: International Conference on Computational Methods in Marine Engineering, CNR, 2015, pp. 58–72.
[10] S.R.K. Nielsen, Q. Zhou, M.M. Kramer, B. Basu, Z. Zhang, Optimal control of nonlinear wave energy point converters, Ocean Eng. 72 (2013) 176–187.
[11] R. Hansen, M.M. Kramer, Modelling and control of the wavestar prototype, In: Proceedings of the 9th European Wave and Tidal Conference, 2011.
[12] R.W.M. Hendrikx, J. Leth, P. Andersen, W.P.M.H. Heemels, Optimal control of a wave energy converter, In: Proceedings of the 2017 IEEE Conference on Control Technology and Applications (CCTA), Kohala Coast, HI, USA, 27–30 August, 2017, pp. 779–786.
[13] J. Hals, J. Falnes, T. Moan, Constrained optimal control of a heaving buoy wave-energy converter, J. Offsh. Mech. Arct. Eng. 133 (1) (2010) 011401.
[14] M. Richter, M.E. Magana, O. Sawodny, T.K.A. Brekken, Nonlinear model predictive control of a point absorber wave energy converter, IEEE Trans. Sustain. Energy 4 (1) (2013) 118–126.
[15] M.N. Soltani, M.T. Sichani, M. Mirzaei, Model predictive control of buoy type wave energy converter, IFAC Proc. Vol. 47 (3) (2014) 11159–11164.
[16] G. Bacelli, J.V. Ringwood, Numerical optimal control of wave energy converters, IEEE Trans. Sustain. Energy 6 (2) (2015) 294–302.
[17] R. Genest, J.V. Ringwood, Receding horizon pseudospectral control for energy maximization with application to wave energy devices, IEEE Trans. Control Syst. Technol. 25 (1) (2017) 29–38.
[18] J.B. Roberts, P.D. Spanos, Random Vibration and Statistical Linearization, Courier Corporation, 2003.
[19] R. Genest, F. Bonnefoy, A.H. Clement, A. Babarit, Effect of non-ideal power take-off on the energy absorption of a reactively controlled one degree of freedom wave energy converter, Appl. Ocean Res. 48 (2014) 236–243.
[20] J. Newman, Marine Hydrodynamics, The MIT Press, 1977.
[21] W. Cummins, The impulse response functions and ship motions, Schiff-stechnik 9 (1962) 101–109.
[22] O. Faltinsen, Sea Loads on Ships and Offshore Structures, Cambridge University Press, 1990.

[23] M. Penalba Retes, G. Giorgi, J. Ringwood, A review of non-linear approaches for wave energy converter modelling., In: Proceedings of the 11th European Wave and Tidal Energy Conference. European Wave and Tidal Energy Conference, 2015.
[24] G. Giorgi, J.V. Ringwood, Comparing nonlinear hydrodynamic forces in heaving point absorbers and oscillating wave surge converters, J. Ocean Eng. Mar. Energy 4 (1) (2018) 25–35.
[25] A.S. Zurkinden, F. Ferri, S. Beatty, J.P. Kofoed, M.M. Kramer, Non-linear numerical modeling and experimental testing of a point absorber wave energy converter, Ocean Eng. 78 (2014) 11–21.
[26] J. Falnes, Ocean Waves and Oscillating Systems: Linear Interactions Including Wave-Energy Extraction, Cambridge University Press, 2002.
[27] WAMIT, WAMIT User Manual, version 7.0. Technical Report, 2011.
[28] S.R.K. Nielsen, Z. Zhang, Stochastic Dynamics, Aarhus Unversity Press, 2017.
[29] D.S. Naidu, Optimal Control Systems, CRC Press, 2002.
[30] N.E. Huang, Z. Shen, S.R. Long, M.C. Wu, H.H. Shih, Q. Zheng, N.C. Yen, C.C. Tung, H.H. Liu, The empirical mode decomposition and the Hilbert spectrum for nonlinear and non-stationary time series analysis, In: Proceedings of the Royal Society of London A: Mathematical, Physical and Engineering Sciences, The Royal Society, 1998.
[31] H. Cramér, M.R. Leadbetter, Stationary and Related Stochastic Processes: Sample Function Properties and Their Applications, Courier Corporation, 2013.
[32] K. Hasselmann, T.P. Barnett, E. Bouws, et al., Measurements of Wind Wave Growth and Swell Decay During the Joint North Sea Project (JONSWAP), Deutches Hydrographisches Institut, 1973.
[33] A.S. El-Bakry, R.A. Tapia, T. Tsuchiya, Y. Zhang, On the formulation and theory of the Newton interior-point method for nonlinear programming, J. Optim. Theory Appl. 89 (3) (1996) 507–541.